Bull. Mater. Sci. (2019) 42:223
https://doi.org/10.1007/s12034-019-1905-2

Hydrothermal synthesis of strontium-doped ZnS nanoparticles: structural, electronic and photocatalytic investigations

R BOULKROUNE[1], M SEBAIS[1], Y MESSAI[2,*], R BOURZAMI[3], M SCHMUTZ[4], C BLANCK[4], O HALIMI[1] and B BOUDINE[1]

[1]Laboratory of Crystallography, Department of Physics, Mentouri Brothers University Constantine 1, Constantine 25000, Algeria
[2]Laboratoire d'Etude des Surfaces et Interfaces de la Matière Solide (LESIMS), Université Badji Mokhtar, Annaba 23000, Algeria
[3]Emerging Materials Research Unit, Ferhat Abbas University Sétif 1, Sétif 19000, Algeria
[4]CNRS, Institut Charles Sadron, Université de Strasbourg, 23 rue du Loess, BP 84047, 67034 Strasbourg Cedex 2, France
*Author for correspondence (messai.youcef@live.fr)

MS received 21 January 2019; accepted 28 March 2019

Abstract. Strontium-doped ZnS nanoparticles (NPs) (1.5, 5 and 9 wt%) were synthesized through a surfactant free hydrothermal method. The structural characterization by X-ray diffraction confirms the synthesis of ZnS, with its two crystalline phases (cubic and hexagonal), without apparition of any peaks related to Sr phases. The crystallite size is affected by Sr doping concentration and was estimated in the range of 2.24–2.51 nm. Furthermore, transmission electron microscopy images show that the NPs have great tendency to aggregate into spherical shapes. Spectroscopy analysis revealed vibration modes specific to ZnS materials on the Raman spectra at about 260 and 345 cm^{-1} and on Fourier-transform infrared spectra at 668.9 cm^{-1}. Electronic investigation performed by UV–Visible diffuse reflectance spectroscopy showed that the synthesized ZnS NPs are optically transparent in the visible domain and their band gap energy decreases from 3.42 to 3.38 eV with increasing Sr concentration. Finally, the methyl orange degradation rate increases with Sr concentration, revealing an improvement in the photocatalytic properties of Sr-doped ZnS NPs.

Keywords. Hydrothermal synthesis; Sr-doped ZnS nanoparticles; photocatalysis.

1. Introduction

The accumulation of organic pollutants in the environment as a result of their intensive use is one of the main causes of ecosystem disruption. Photocatalysis is an inexpensive and effective technique for solving this problem. Scientific research is therefore focussed on the production of new environmentally friendly and inexpensive materials for the removal of these pollutants. Semiconductor nanostructures have shown some efficiency owing to their interesting chemical and physical properties [1,2].

Indeed, the electronic properties of nanocrystals change when their size becomes very small due to the quantum confined effect [3–5]. Moreover, the high surface-to-volume ratio and the prominent role played by the atomic surface arrangement improve significant optical, electrical and chemical properties and particularly catalysis and photocatalysis [6].

Various semiconductors have been studied for the treatment of environmental pollution. Among the most used are metal oxides such as TiO_2 [7], ZnO [8], SnO_2 [9] and other compounds of group II–VI such as CdS [10], ZnSe [11], CdTe [12], HgS [13] and ZnS [14].

Zinc sulphide (ZnS) is an important compound of the II–VI group because of its wide direct band gap and large excitation energy (39 meV) [15]. Owing to its optical, electrical and luminescence properties, ZnS is widely used in several kinds of applications such as light emitting diodes, flat panel displays, UV-sensors, chemical sensors, biosensors [16] and solar cells [17]. It is also used in the domain of the photocatalysis [18] due to its high-chemical stability.

Several methods have been employed to synthesize ZnS nanoparticles (NPs) such as sol–gel [19], precipitation [20], solvothermal [21] and microemulsion-hydrothermal method [22]. ZnS is found in two distinct crystalline phases: zinc-blende (cubic phase) and wurtzite (hexagonal phase), with

Electronic supplementary material: The online version of this article (https://doi.org/10.1007/s12034-019-1905-2) contains supplementary material, which is available to authorized users.

Published online: 02 July 2019

direct band gap energies of 3.72 and 3.77 eV, respectively [15].

The doping of ZnS with foreign elements can improve its properties and particularly the photocatalytic efficiency; indeed, the doping introduces new levels in the forbidden band that could act as traps for photo-generated electron–hole pairs, thus reducing their recombination rate. ZnS doped by transition metal ions has been reported in many studies such as Mn [23], Co [24], Cu [25], Fe [26] and Ni [27] as well as metal ion Pb [28]. The doped materials show important optical and luminescence properties, owing to their crucial role in the change of the electronic structure and increase in electron transition probabilities of the host material. Also, the effects on the physical properties of rare-earth ion-doped ZnS NPs are reported: Sm^{+3} [29], Tb^{+3} [30], Eu^{+3} [31] and Er^{+3} [32].

In this study, the alkaline earth metal strontium (Sr) was used to dope a ZnS semiconductor and test its ability to improve photocatalytic properties. Indeed, the ionic radius of Sr^{2+} (1.18 Å) being larger than that of Zn^{2+} (0.74 Å) and the electronic structure mismatch of the cations could induce important defects in the crystal structure which would modify the optical properties and consequently the photocatalytic properties which are closely related to them. Also, according to the references [33,34] Sr-doped ZnO crystallites were found to have enhanced photocatalytic activity compared to pure ZnO; so we also expect to observe an improvement in the photocatalytic degradation of methyl orange (MO) by Sr-doped ZnS NPs. Furthermore, to the best of our knowledge, no reports are available in the literature on the study of the photocatalytic activity of Sr-doped ZnS NPs.

To perform this study, Sr-doped ZnS NPs with different concentrations were synthesized by the hydrothermal method; the prepared NPs were characterized by X-ray diffraction (XRD), transmission electron microscopy (TEM), UV–Visible diffuse reflectance, Fourier-transform infrared (FTIR) and Raman spectroscopy. Finally, the photocatalytic activities of the Sr-doped NPs are evaluated in the degradation of well-known organic dye MO, an important pollutant in the dyeing industry.

2. Materials and methods

2.1 *Synthesis of undoped and Sr-doped ZnS NPs*

NPs were synthesized through a surfactant free hydrothermal method using zinc acetate dihydrate ($Zn(CH_3COO)_2 \cdot 2H_2O$) and thiourea ($SC(NH_2)_2$) as starting materials; 6.5 mmol of each precursor were separately dissolved in 65 ml of distilled water at room temperature under magnetic stirring for about 45 min, until complete dissolution. The above two prepared solutions were then mixed under stirring by adding the thiourea solution dropwise into the zinc acetate solution. Sr-Doped ZnS NPs with different concentrations (1.5, 5 and 9 wt%) were synthesized by adding the specified amount of strontium chloride hexahydrate ($SrCl_2 \cdot 6H_2O$) into the above mixture under magnetic stirring for 20 min. The final mixture was then transferred into a 190 ml Teflon-lined stainless steel autoclave. Thermal treatment was performed in an electric oven at 140°C for 7 h. Once the reaction being completed, the autoclave was cooled down to room temperature. The produced powder was washed several times with distilled water and ethanol in order to remove the residual impurities, and then dried in air at 50°C for 2 h. The samples were respectively labelled as: ZnS, ZnS:Sr1.5%, ZnS:Sr5% and ZnS:Sr9%.

2.2 *Characterization techniques*

The synthesized NPs have been characterized by various techniques. The results of structural, optical, vibrational and morphological characterization of Sr-doped ZnS NPs was compared with those of undoped-ZnS NPs. The crystalline structures were investigated with a PANalytical X'Pert PRO diffractometer in the range of 20−70°, using CuKα radiation (λ = 1.5406 Å, 40 mA, 45 kV). The optical spectra were recorded using a UV–Visible diffuse reflectance spectrometer (JASCO V-750) equipped with an integrating sphere model ILN-725. The vibrational properties were determined by a FT-IR spectroscopy technique, using a JASCO-FTIR-4200 spectrophotometer. Raman spectroscopy investigation was carried out using a Senterra type Bruker spectrometer equipped with a 532 nm laser, providing the excitation wavelength. The TEM and high-resolution transmission electron microscopy (HRTEM) images were recorded using a Tecnai G2 20 Twin instrument.

2.3 *Photocatalytic activity measurement*

The photocatalytic degradation of MO under UV irradiation was used to evaluate the photocatalytic activity of the undoped and Sr-doped ZnS NPs. A monochromatic UV lamp (Vilber Lourmat VL-215-BL 2 × 15 W) emitting at 365 nm was used as the irradiation source during the photocatalytic degradation. The light intensity reaching the surface of aqueous dye solution was ∼2600 μW cm^{-2}. For the experiments, a suspension of 7 mg of ZnS NPs in water was exposed to ultrasonic waves for 10 min to disperse NPs; this suspension was then added to the MO stock solution to obtain 10 ml of aqueous MO solution (5.10–5 M) which was placed in a double walled flask and kept at 25°C by a water cooling system. The area of aqueous dye solution exposed to light was about 28 cm^2.

Firstly, to estimate the adsorption rate, the absorption of MO was measured after 30 min of stirring with NPs in the dark to ensure complete equilibrium of adsorption/desorption of MO on the ZnS NP surface. It was only about 7%, negligible compared to the removal of MO under UV irradiation.

The experimental data of photocatalysis illustrate the decay of the absorbance recorded at the characteristic absorption peak of MO (λ = 464 nm) and normalized to the value obtained prior to the first illumination.

3. Results and discussion

3.1 *XRD analysis*

Figure 1 shows the XRD patterns of the synthesized undoped and Sr-doped ZnS NPs. The peaks observed at the 2θ angular positions of 29.21, 32.97, 48.77 and 57.65° correspond to reflections from (111), (200), (220) and (311) crystallographic planes of the zinc-blende (cubic) phase of the ZnS compound according to JCPDS card 05-0566. The two weak peaks (shoulders), at $2\theta = 27°$ and 30.6°, attributed to reflections from (002) and (101) crystallographic planes of the wurtzite (hexagonal) phase of ZnS according to JCPDS card 03-1093, indicate that the synthesized ZnS products contribute to a small amount in the wurtzite structure. All observed peaks belong to ZnS phases and there are no detected peaks for the phases of Sr^{2+} element. This result means that Sr^{2+} ions are incorporated into the crystallographic sites of Zn^{2+} ions. A similar result reported that the doping with Sr^{+2} has no effect on the crystallographic phase of ZnO [33] and TiO_2 [35].

For the cubic system, the lattice parameter a is related to the interplanar distance d_{hkl} as follows:

$$d_{hkl} = \frac{a}{\sqrt{h^2 + k^2 + l^2}}, \tag{1}$$

where h, k and l are Miller indices of the Bragg planes. From the XRD patterns, a slight shift in the peak positions is observed for the Sr-doped samples compared to the undoped-ZnS NPs, denoting a weak change in the lattice parameters (5.27–5.30 Å) due to the incorporation of larger Sr^{2+} replacing Zn^{2+} in the ZnS lattice [36–38].

The crystallite size was estimated using the well-known Debye–Scherrer's formula:

$$D = \frac{0.94\lambda}{\beta \cos\theta}, \tag{2}$$

where λ is the X-ray wavelength (1.54056 Å), β is the full-width at half maximum of the peak and θ is the diffraction angle.

The estimated crystallite sizes of Sr-doped ZnS NPs with concentrations of 0, 1.5, 5 and 9% are 2.24, 2.34, 2.46 and 2.51 nm, respectively. This result means that doping with Sr^{2+} ions promotes the growth of ZnS NPs.

3.2 *FT-IR analysis*

The FT-IR spectra of Sr-doped ZnS NPs recorded in the range of 4000–600 cm^{-1} are shown in figure 2. The peak located at 668.9 cm^{-1} is attributed to the stretching vibration of the Zn–S bond [39,40], which confirms the synthesis of ZnS NPs. The spectral band at 2955 cm^{-1} is attributed to C–H stretching vibrations [41]. Furthermore, the peak observed at 1630 cm^{-1} is assigned to the bending vibrations of the absorbed water molecules [42], whereas the peak positioned at 1399 cm^{-1} could be attributed to carboxyl and methylene groups.

3.3 *Raman spectroscopy*

Raman scattering is a powerful probe to illustrate the effects on crystalline structures caused by ion incorporation. Figure 3 shows the Raman spectra of undoped and Sr-doped nanostructured ZnS samples. The spectra exhibit broad peaks at 71, 94, 145, 260, 345 and 465 cm^{-1}.

From the literature, we note that different frequencies are reported for vibration modes of both cubic and hexagonal structures of the ZnS semiconductor. Generally, the positions of peaks on Raman spectra are shifted toward lower or higher frequencies as they are often affected by the size and morphology of crystallites, by the nature and concentration of chemical dopants, by the type of defects and created strains and finally by the used excitation wavelength. These factors cause variations in the frequencies of lattice vibrations which

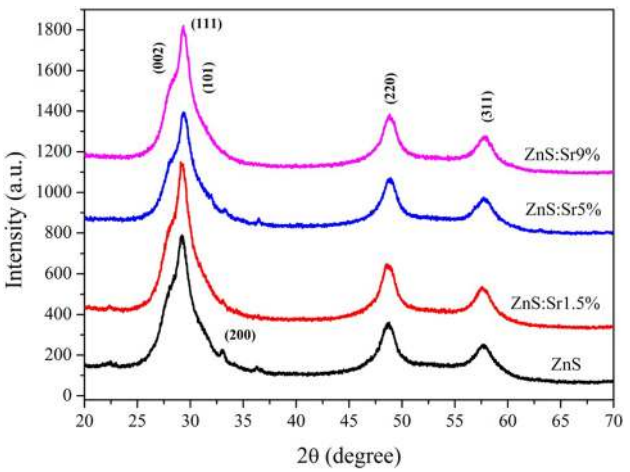

Figure 1. XRD patterns of undoped and Sr-doped ZnS NPs.

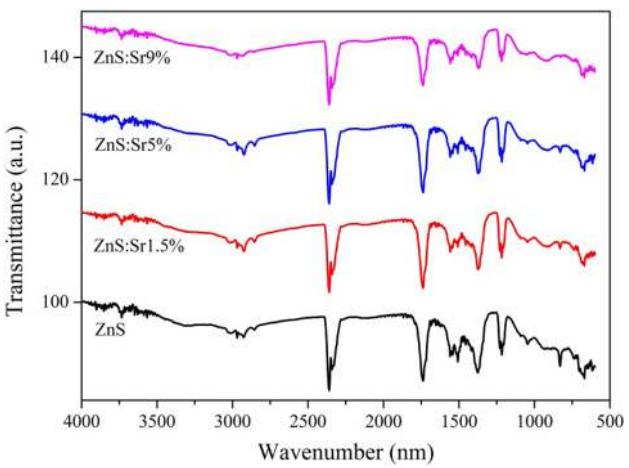

Figure 2. FT-IR spectra of undoped and Sr-doped ZnS NPs.

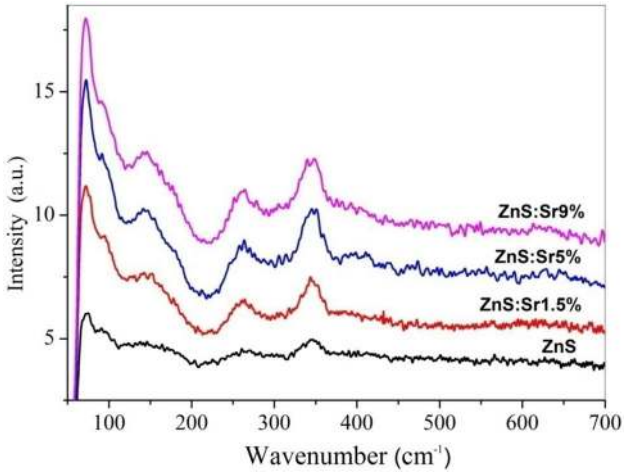

Figure 3. Raman spectra of undoped and Sr-doped ZnS NPs.

lead to some discrepancies in the assignment of vibration modes [43–46].

First order Raman spectra of bulk hexagonal and cubic phases of the ZnS semiconductor have been reported by many authors [47,48]. They have observed that the transverse optical (TO) phonon modes (A1 and E1 symmetry) and the longitudinal optical (LO) phonon modes (A1 and E1 symmetry) of cubic ZnS crystals are situated at around 275 and 350 cm^{-1}, respectively. The two E2 modes of hexagonal ZnS are located at around 72 and 285 cm^{-1}.

Also, for the second-order Raman modes, there are some discrepancies in the reported values of frequencies and in assignment of modes because of the rate of disorder in the symmetry of the crystal structure. For example, modes at 94 and 145 cm^{-1} can be related to the smallness of ZnS nanocrystallites [49] for which the selection rules are broken. The peaks at 260 and 465 cm^{-1} correspond to the second-order Raman modes of ZnS cubic and hexagonal structures, respectively [50].

Comparing the frequencies reported in the literature with those measured, we can deduce that the samples are formed with both cubic and hexagonal phases of ZnS as illustrated by XRD analysis. The experimental results are close to previous reports with slight deviations due to difference in techniques of synthesis, created strains in the crystal lattice and size of crystallites [50]. The nanometric size of synthesized-ZnS nanocrystallites (table 1) has a phonon confinement effect [22,51] which is reflected by a broadening and an intensity increase of Raman peaks (figure 3). Moreover, the structure deformation induced by doping results in an increase in the TO and LO peak intensity; a similar result was observed for Al-doped ZnS NPs [43].

3.4 *Electronic properties*

The electronic properties of undoped and Sr-doped ZnS NPs were analysed with the aim at evaluating the doping effect on the optical absorption and the band gap energy. The recorded UV–Visible absorption spectra are depicted in figure 4. It is shown that all NPs are almost transparent in the visible region and exhibit a strong absorption in the UV region. The maximum absorption is located at around 334 nm for all ZnS NPs. A slight shift towards higher wavelength is observed for the absorption edge of Sr-doped ZnS samples. This expresses a decrease in the band gap energy of Sr-doped ZnS NPs which is a favourable factor for the improvement of photocatalytic performances.

Table 1. Band gap energy and Urbach energy at different doping rates.

Samples	E_g (eV)	E_U (meV)
ZnS	3.42	75
ZnS-1.5%Sr	3.40	80
ZnS-5%Sr	3.39	109
ZnS-9%Sr	3.38	121

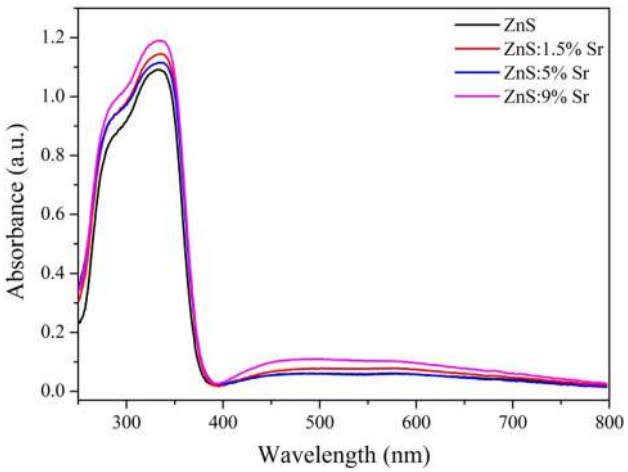

Figure 4. UV–Visible absorbance spectra of undoped and Sr-doped ZnS NPs.

For the estimation of the band gap energy E_g, the absorption coefficient $F(R)$ is deduced from the reflectance curves according to the Kubelka–Munk equation [52]:

$$F(R) = \frac{(1-R)^2}{2R}, \tag{3}$$

where R is the reflectance and $F(R)$ is equivalent to the absorption coefficient α.

The band gap energy E_g has been determined using the Tauc relation [53]:

$$(F(R)\,h\nu)^2 = A\left(h\nu - E_g\right). \tag{4}$$

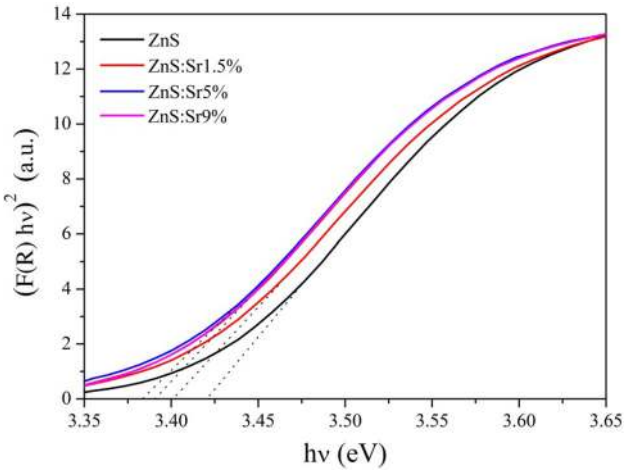

Figure 5. Evolution of band gap energy E_g, according to the Kubelka–Munk approach.

The extrapolation of the linear part of Tauc plots intersects with the photon energy axis to define E_g (figure 5).

The band gap energy of the undoped sample is estimated to be 3.42 eV. However, the band gap energy for the doped samples is decreased to 3.38 eV by increasing the Sr concentration (table 1). A comparable result was obtained in Sr-doped SnO_2 [54].

From the absorption spectra shown in figure 4, we observe that the tails of the absorption have been increased in the visible region with Sr-doping. This phenomenon is attributed to the generation of additional energy states within the band gap which create band tails extending the valence and conduction band edges. The formation of defect states in the band gap allows a reduction of the recombination rate of photo-generated electron–hole pairs because charge transitions occur through defects; such hypothesis was earlier reported in references [10,11,55]. This low-recombination rate leads to an enhancement of photocatalytic activity.

This change in the electronic structure can be estimated by the Urbach energy E_U according to the following relation [56]:

$$\alpha = \alpha_0 \exp\left(\frac{h\nu - E_0}{E_U}\right), \tag{5}$$

where α_0 and E_0 are two constants related to the material.

E_U is determined by plotting the logarithm of the absorption coefficient α (or $F(R)$ in our case) as a function of $h\nu$. The inverse of the slope of the linear part of curves is equal to the Urbach energy E_U. The increase in the E_U value and the decrease in the E_g value with increasing Sr concentration (table 1) are attributed to the formation of defect states near the conduction band, causing further reduction in the optical band gap. A comparative result was observed by Raghavendra *et al* [37] who reported that Sr-doping of ZnO induces a decrease in the band gap energy. Similar observation was also reported in the case of Cd-doped ZnO [57].

3.5 *TEM micrograph analysis*

Figure 6a shows the TEM image for undoped-ZnS NPs (the images of Sr-doped ZnS NPs with different percentages are shown in supplementary figure S1). The NPs agglomerate into spherical shaped aggregates, which make them difficult to observe primary particles. The aggregate size distribution is obtained from the TEM image, and it is fitted with a Gaussian function [56]:

$$Y = Y_0 + \frac{A}{w\sqrt{\pi/2}} e^{-2((x-x_c)^2/w^2)}, \tag{6}$$

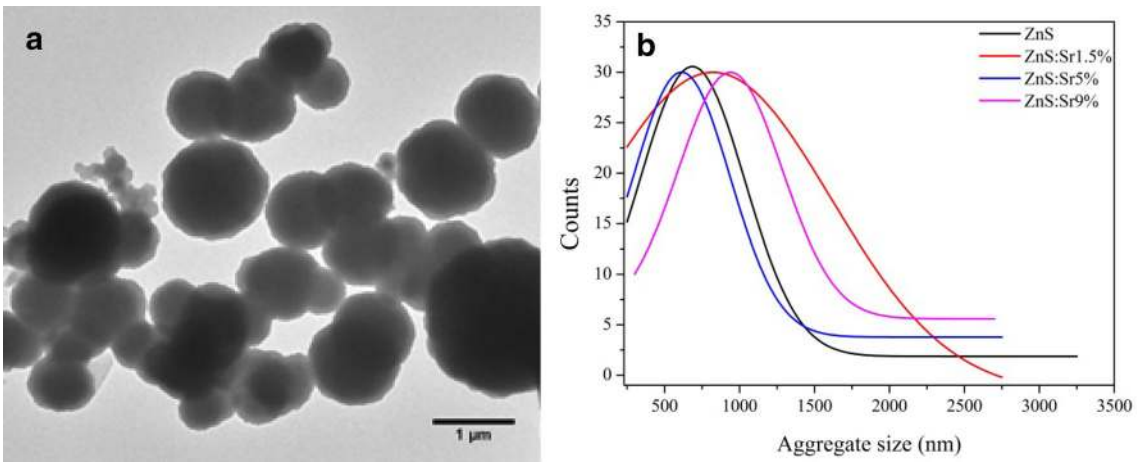

Figure 6. (**a**) TEM image of ZnS NPs and (**b**) size distribution obtained from TEM images of undoped and Sr-doped ZnS NPs.

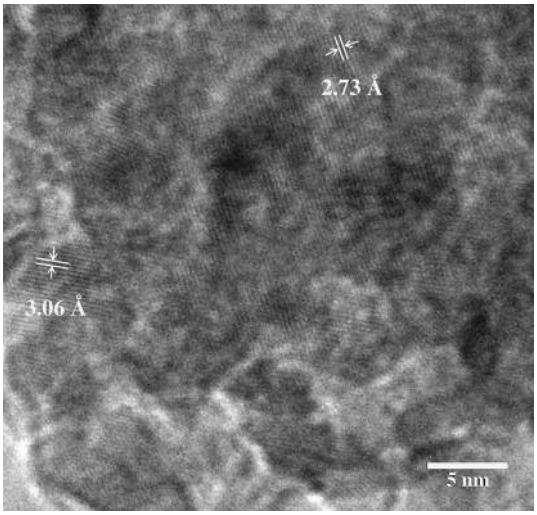

Figure 7. HRTEM image of the ZnS:Sr1.5% NPs.

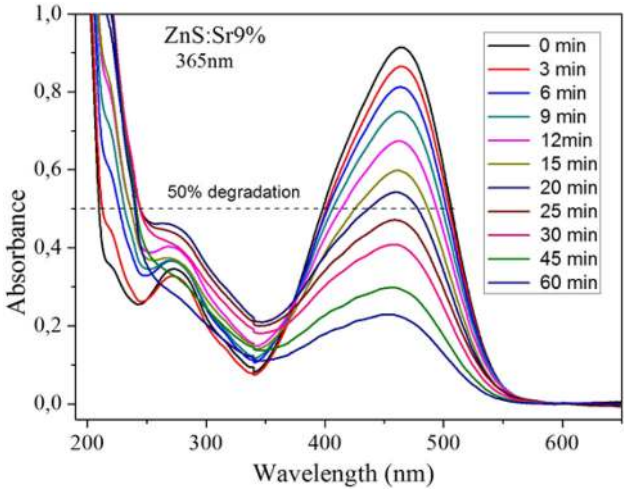

Figure 8. UV–Vis absorbance spectra of aqueous MO solution in the presence of ZnS:Sr9% NPs under UV irradiation at different intervals of time.

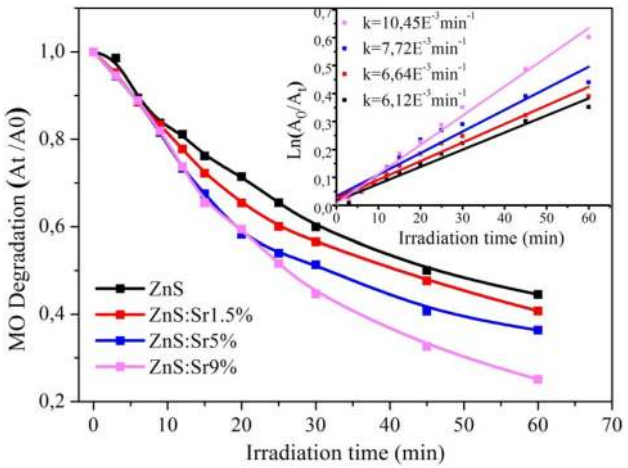

Figure 9. Photocatalytic degradation of MO under UV irradiation with undoped and Sr-doped ZnS NPs.

where Y_0 is the offset, A is the area, w is the width and x_c is the centre position of the Gaussian curve. The obtained aggregate average sizes of 684, 824, 614 and 938 nm correspond to ZnS, ZnS:Sr1.5%, ZnS:Sr5% and ZnS:Sr9% samples, respectively. Moreover, the ZnS:Sr1.5% NPs have the highest tendency for aggregation, forming a large Gaussian function shifted to the high-size values (figure 6b).

Figure 7 shows the HRTEM image of the ZnS:Sr1.5% sample. The clearly observed lattice fringes indicate that the particles are crystalline. The measured interplanar distances 3.05 and 2.73 Å correspond to the inter-reticular spacing between (111) planes and (200) planes of the cubic phase, respectively [58]. These two planes were also observed at the angular positions of 29.21 and 32.97° on the XRD patterns.

3.6 *Photocatalytic activity of undoped and Sr-doped ZnS NPs*

The semiconductors, when activated by photons with sufficient energy, will generate electron–hole pairs by excitation of electrons from the valence band to conduction band. The migration of photo-generated carriers to the photocatalyst surface will produce, within redox reactions, reactive oxygen species such as hydroxyl $OH^{\bullet}$, superoxide $O_2^{\bullet -}$ and H_2O_2, that are the most responsible for the degradation of several organic pollutants.

Figure 8 displays the UV–Vis absorption spectra of the aqueous MO solution in the presence of ZnS:Sr9% NPs under exposure to UV irradiation for different intervals of time. The intensity of the absorption peak of MO at 464 nm decreases with increase in the irradiation time which indicates the degradation of MO dye by photocatalysis. On these spectra no new absorption band appears and this means the absence of byproduct formation.

Figure 9 shows the degradation rate of MO under UV irradiation in the presence of the synthesized NPs. The Sr-doped ZnS NPs reduced the MO concentration faster than the undoped-ZnS NPs. It was observed that about 50% of MO was degraded within 45 min by the undoped-ZnS NPs, while it took 26 min for the ZnS:Sr9% NPs. This improvement may be explained by the decrease in the band gap energy (E_g) values after doping (table 1). Indeed, the created energy levels in the band gap induce an increase in the number of electron–hole pairs on the surface of NPs whose existence and evolution influence the photocatalytic activity. Also, a larger surface area could provide more active sites for reactant molecules and promote the efficiency of the photocatalysis. On the other hand, the energy of the irradiation wavelength (365 nm/3.39 eV) can generate less electron–hole pairs for the ZnS and ZnS:Sr1.5% samples of which the band gap energy is higher. We can say that the size effect of the NPs on the photocatalytic activity is almost the same for all samples because the surface

of the NPs in contact with the MO solution is substantially constant as the size of the NPs varies very little.

The inset of figure 9 shows fitted data by a pseudo first-order reaction model given by the following equation [59]:

$$\ln(A_0/A_t) = k \cdot t, \tag{7}$$

where A_0 is the initial absorbance of the dye solution before the irradiation process is started, A_t is the absorbance after the irradiation time t and k is the rate constant. The rate constants were found to be 6.12×10^{-3}, 6.64×10^{-3}, 7.72×10^{-3} and 10.45×10^{-3} min^{-1} for ZnS, ZnS:Sr1.5%, ZnS:Sr5% and ZnS:Sr9% samples, respectively; the highest rate constant value corresponds to the highest doping concentration.

The degradation rate of MO obtained by the synthesized samples (75% in 60 min) can be considered as a good result with regard to that of Cr-doped ZnS (65% in 5 h) [60] or Mn-doped ZnS (70% in 120 min) [61].

4. Conclusion

Undoped and Sr-doped ZnS NPs were successfully synthesized through a surfactant free hydrothermal method. The structural, morphological, optical and photocatalytic properties of the samples were systematically studied.

The structural investigation carried out by XRD reveals that ZnS NPs crystallize in both cubic and hexagonal phases, with a small change in the lattice parameter of ZnS, confirming Sr incorporation into Zn sites, inducing an increase in the crystallite size. Raman spectroscopy confirms the synthesis of the ZnS NPs and the presence of cubic and hexagonal phases. Furthermore, the TEM illustrates that the NPs have a high tendency for aggregation, forming spherical shapes. The optical band gap of Sr-doped ZnS NPs decreased from 3.42 to 3.38 eV with increasing Sr concentration. Photocatalytic measurements showed a significant degradation of MO dye by Sr-doped ZnS NPs. The rate of degradation was found to fit first-order reaction kinetics with the highest rate constant value of 1.045×10^{-2} min^{-1} obtained for the ZnS:Sr9% sample.

Finally, the photocatalytic study showed that the synthesized Sr-doped ZnS NPs have improved photocatalytic properties which make them potential candidates for organic dye degradation.

Acknowledgements

The authors are grateful to the staff of the electronic microscopy platform of the Institut Charles Sadron of the Université de Strasbourg for their help in performing the TEM and HRTEM images. The authors thank Mr Grine Sami for his assistance in photocatalytic experiments and are grateful to the Algerian Ministry of Higher Education and Scientific Research for his support of this work.

References

[1] Chong M N, Jin B, Chow CWK and Saint C 2010 *Water Res.* **44** 2997
[2] Chakrabarti S and Dutta B K 2004 *J. Hazard. Mater.* **B112** 269
[3] Jiang J, Oberdörster G and Biswas P 2009 *J. Nanoparticle Res.* **11** 77
[4] Genzel L and Martin T P 1972 *Phys. Status Solidi B* **51** 91
[5] Ruppin R and Englman R 1970 *Rep. Prog. Phys.* **33** 149
[6] Toennies J P, Benedek G, Martin T P and Pacchioni G 1987 *Elemental and Molecular Clusters Proceedings of the 13th International School*, Erice, Italy, July 1–15
[7] Lan Y, Lu Y and Ren Z 2013 *Nano Energy* **2** 1031
[8] Ong C B, Ng L Y and Mohammad A W 2018 *Renew. Sustain. Energy Rev.* **81** 536
[9] Mishra M K, Singh N, Pandey V and Haque F Z 2016 *J. Adv. Phys.* **5** 8
[10] Cheng L, Xiang Q, Liao Y and Zhang H 2018 *Energy Environ. Sci.* **11** 1362
[11] Bo F, Jian C, Donglai H, Hongtao L, Shuo Y, Xiuyan L *et al* 2014 *Mater. Sci. Semicond. Process.* **27** 865
[12] Wang X, Ma Q, Li B, Li Y and Su X 2007 *Lumin. J. Biol.Chem. Lumin.* **22** 1
[13] Patel B K, Rath S, Sarangi S N and Sahu S N 2007 *Appl. Phys. A* **86** 447
[14] Díaz-Reyes J, Castillo-Ojeda R S, Sánchez-Espíndola R, Galván-Arellano M and Zaca-Morán O 2015 *Curr. Appl. Phys.* **15** 103
[15] Fang X, Zhai T, Li L, Wua L, Bando Y, Golberg D *et al* 2011 *Prog. Mater. Sci.* **56** 175
[16] Navneet K, Sukhmeen K, Jagpreet S and Mohit R 2016 *J. Bioelectron. Nanotechnol.* **1** 1
[17] Ummartyotin S and Infahsaeng Y 2016 *Renew. Sustain. Energy Rev.* **55** 17
[18] Lee G-J and Wu J J 2017 *Powder Technol.* **318** 8
[19] Stanic V, Etsell T H, Pierre A C and Mikula R J 1997 *Mater. Lett.* **31** 35
[20] Ramasamy V, Praba K and Murugadoss G 2012 *Spectrochim. Acta A Mol. Biomol. Spectrosc.* **96** 963
[21] La Porta F A, Ferrer M M, Longo V M, Sambrano J R, Longo E, Andrés J *et al* 2013 *J. Alloys Compd.* **556** 153
[22] Yang R D, Tripathy S, Tay F E H, Gan L M and Chua S J 2003 *J. Vac. Sci. Technol.* **21** 984
[23] Murugadoss G 2011 *J. Lumin.* **131** 2216
[24] Salem J K, Hammad T M, Kuhn S, Draaz M A, Hejazy N K and Hempelmann R 2014 *J. Mater. Sci.: Mater. Electron.* **25** 2177
[25] Sun L, Liu C, Liao C and Yan C 1999 *J. Mater. Chem.* **9** 1655
[26] Saikia D, Raland R and Borah J P 2016 *Phys. E Low-Dimens. Syst. Nanostructures* **83** 56
[27] Borse P H,Vogel W and Kulkarni S K 2006 *J. Colloid Interface Sci.* **293** 437
[28] Yang P, Lü M, Xü D, Yuan D, Chang J, Zhou G *et al* 2002 *Appl. Phys. Mater. Sci. Process.* **74** 257
[29] Kushida T, Kurita A, Watanabe M, Kanematsu Y, Hirata K, Okubo N *et al* 2000 *J. Lumin.* **87–89** 466
[30] Ramu S and Vijayalakshmi R P 2017 *J. Supercond. Nov. Magn.* **30** 1921
[31] Ashwini K, Pandurangappa C and Nagabhushana B M 2012 *Phys. Scr.* **85** 065706

[32] Ahmadi M, Javadpour S, Khosravi A and Gharavi A 2008 *Jpn. J. Appl. Phys.* **47** 5089
[33] Yousefi R, Sheini F J, Cheraghizade M, Gandomani S K, Sáaedi A, Azarang M *et al* 2015 *Mater. Sci. Semicond. Process.* **32** 152
[34] Lakshmana Perumal S, Hemalatha P, Alagar M and Navaneetha Pandiyaraj K 2015 *Int. J. Chem. Phys. Sci.* **4** IJCPS Special Issue ETP
[35] Mehnane H F, Wang C, Yu W, Sun W, Liu H, Bai S *et al* 2017 *RSC Adv.* **7** 2358
[36] Udayabhaskar R and Karthikeyan B 2014 *J. Appl. Phys.* **116** 094310
[37] Raghavendra P V, Bhat J S and Deshpande N G 2017 *Mater. Sci. Semicond. Process.* **68** 262
[38] Shannon R D 1976 *Acta Crystallogr. A* **32** 751
[39] Thangavel S, Krishnamoorthy K, Kim S-J and Venugopal G 2016 *J. Alloys Compd.* **683** 456
[40] Chen J, Zhu Y and Zhang Y 2016 *Spectrochim. Acta A Mol. Biomol. Spectrosc.* **164** 98
[41] Shanmugam N, Cholan S, Kannadasan N, Sathishkumar K and Viruthagiri G 2014 *Solid State Sci.* **28** 55
[42] Jothibas M, Jeyakumar S J, Manoharan C, Punithavathy I K, Praveen P and Richard J P 2017 *J. Mater. Sci.: Mater. Electron.* **28** 1889
[43] Amaranatha Reddy D, Liu C, Vijayalakshmi R P and Reddy B K 2014 *J. Alloys Compd.* **582** 257
[44] Acharya S A, Maheshwari N, Laxman T, Anjali K and Kulkarni S K 2013 *Cryst. Growth Des.* **13** 1369
[45] Rani G and Sahare P D 2013 *Spectrosc. Lett.* **46** 391
[46] Lan C, Hong K, Wang W and Wang G 2003 *Solid State Commun.* **125** 455
[47] Arguello C A, Rousseau D L and Porto S P S 1969 *Phys. Rev.* **181** 1351
[48] Brafman O and Mittra S S 1968 *Phys. Rev.* **171** 931
[49] Abdulkbadar M and Thomas B 1995 *Nanostructured Mater.* **3** 289
[50] Cheng Y C, Jin C Q, Gao F, Wu X L, Zhong W, Li S H *et al* 2009 *J. Appl. Phys.* **106** 123505
[51] Aswaghosh L, Manoharan and Jaya N V 2016 *Phys. Chem. Chem. Phys.* **18** 5995
[52] Kortüm G 1969 Reflectance Spectroscopy: Principles, Methods, Applications Springer Science & Business Media Springer-Verlag New York Inc.
[53] Bhatt R, Bhaumik I, Ganesamoorthy S, Karnal A K, Swami M K, Patel H S *et al* 2012 *Phys. Status Solidi* **209** 176
[54] Prabha D, Ilangovan S, Balamurugan S, Suganya M, Anitha S, Nagarethinam V S *et al* 2017 *Opt.- Int. J. Light Electron Opt.* **142** 301
[55] Reber J F and Rusek M 1986 *J. Phys. Chem.* **90** 824
[56] Messai Y, Vileno B, Martel D, Turek P and Mekki D E 2018 *Bull. Mater. Sci.* **41** 41
[57] Gruber T, Kirchner C, Kling R, Reuss F, Waag A, Bertram F *et al* 2003 *Appl. Phys. Lett.* **83** 3290
[58] Bujnakova Z, Balaz M, Zduriencıkova M, Sedlak J, Caplovicova M, Caplovic L *et al* 2017 *Mater. Sci. Eng. C* **71** 541
[59] Muruganandham M and Swaminathan M 2004 *J. Dyes Pigments* **62** 269
[60] Eyasu A, Yadav O P and Bachheti R K 2013 *Int. J. ChemTech Res.* **5** 1452
[61] Joicy S, Saravanan R, Prabhu D, Ponpandian N and Thangadurai P 2014 *RSC Adv.* **4** 44592